Magnetic Frustration in a Quantum Spin Chain: The Case of Linarite $PbCuSO_4(OH)_2$

B. Willenberg,[1,2] M. Schäpers,[3] K. C. Rule,[1] S. Süllow,[2] M. Reehuis,[1] H. Ryll,[1] B. Klemke,[1] K. Kiefer,[1] W. Schottenhamel,[3] B. Büchner,[3] B. Ouladdiaf,[4] M. Uhlarz,[5] R. Beyer,[5] J. Wosnitza,[5] and A. U. B. Wolter[3]

[1]*Helmholtz Center Berlin for Materials and Energy, D-14109 Berlin, Germany*
[2]*Institute for Condensed Matter Physics, TU Braunschweig, D-38106 Braunschweig, Germany*
[3]*Leibniz Institute for Solid State and Materials Research IFW Dresden, D-01171 Dresden, Germany*
[4]*Institute Laue-Langevin, 38042 Grenoble Cedex, France*
[5]*Dresden High Magnetic Field Laboratory, Helmholtz-Zentrum Dresden-Rossendorf, D-01314 Dresden, Germany*

(Received 17 November 2011; published 16 March 2012)

We present a combined neutron diffraction and bulk thermodynamic study of the natural mineral linarite $PbCuSO_4(OH)_2$, this way establishing the nature of the ground-state magnetic order. An incommensurate magnetic ordering with a propagation vector $\boldsymbol{k} = (0, 0.186, \frac{1}{2})$ was found below $T_N = 2.8$ K in a zero magnetic field. The analysis of the neutron diffraction data yields an elliptical helical structure, where one component ($0.638\mu_B$) is in the monoclinic ac plane forming an angle with the a axis of 27(2)°, while the other component ($0.833\mu_B$) points along the b axis. From a detailed thermodynamic study of bulk linarite in magnetic fields up to 12 T, applied along the chain direction, a very rich magnetic phase diagram is established, with multiple field-induced phases, and possibly short-range-order effects occurring in high fields. Our data establish linarite as a model compound of the frustrated one-dimensional spin chain, with ferromagnetic nearest-neighbor and antiferromagnetic next-nearest-neighbor interactions. Long-range magnetic order is brought about by interchain coupling 1 order of magnitude smaller than the intrachain coupling.

DOI: 10.1103/PhysRevLett.108.117202 PACS numbers: 75.10.Jm, 75.25.−j, 75.30.Kz, 75.40.Cx

Frustrated low-dimensional quantum spin systems have attracted great interest in the past years owing to their rich and varied magnetic properties [1,2]. Depending on dimensionality and frustration of the magnetic couplings, a multitude of exotic phases occurs, including, for instance, nematic or multipolar phases in one dimension [3–6] or spin liquids in two dimensions [7,8]. In this field, a major focus lies on the study of strong quantum fluctuations in one-dimensionally coupled frustrated spin systems, which might destabilize classical ground states and give rise to novel phenomena such as multiferroicity for spiral spin states [3–5,9–11].

Particularly in natural minerals, copper oxides have shown intriguing properties with respect to magnetic frustration and low dimensionality [12–16]. Magnetism in these materials arises from the spin $S = 1/2$ moments of the Cu^{2+} ions, and the magnetic couplings vary strongly in magnitude and sign depending on the actual geometry and environment of the copper oxide bonds involved.

One of the most basic models accounting for one-dimensional frustrated quantum spin magnetism considers a competing ferromagnetic nearest-neighbor interaction $J_1 > 0$ and an antiferromagnetic next-nearest-neighbor interaction $J_2 < 0$ between spins $\mathbf{S}_l$, $\mathbf{S}_{l+1}$, and $\mathbf{S}_{l+2}$ (abbreviated FM-AFM systems) in an external field h, described by the Hamiltonian

$$\hat{H} = J_1 \sum_l [\mathbf{S}_l \cdot \mathbf{S}_{l+1}] + J_2 \sum_l [\mathbf{S}_l \cdot \mathbf{S}_{l+2}] - h \sum_l S_l^z. \quad (1)$$

Already for this model, various ground states are predicted depending on the ratio $\alpha = J_2/J_1$. In the limit of a classical isotropic spin model, the ground state is ferromagnetic for a ratio $\alpha > -\frac{1}{4}$, while for $\alpha < -\frac{1}{4}$ it will be incommensurate [17,18]. Recently, Furukawa, Sato, and Onoda [11] predicted even more exotic ground states for this model by taking into account both the effect of quantum fluctuations and local anisotropy. Most importantly, they conclude that—depending on the anisotropy—the region $\alpha < -\frac{1}{4}$ contains chiral ordered states as well as dimerized and Tomonaga-Luttinger liquid phases. Furthermore, by applying a magnetic field, a variety of exotic phases like vector-chiral, spin-nematic, or higher-order polar phases ought to be induced [3,6,19–21].

Experimental realizations of the Hamiltonian given in Eq. (1) include the systems $LiCuVO_4$, $Rb_2Cu_2Mo_3O_{12}$, $LiCu_2O_2$, $NaCu_2O_2$, and Li_2ZrCuO_4 [22–27]. Unfortunately, these materials either have very high saturation fields or are not available as single crystals. Hence, many experimental tests of theoretical modelings of Eq. (1) are lacking. Only the natural mineral linarite $PbCuSO_4(OH)_2$ conforms to the FM-AFM model, combining an accessible saturation field of ~10 T with the availability of single crystals [13–15], thus allowing easy experimental studies of this model in the field range up to saturation.

Linarite crystallizes in a monoclinic lattice (space group $P2_1/m$; $a = 9.682$ Å, $b = 5.646$ Å, $c = 4.683$ Å, and $\beta = 102.65°$ [28]), with buckled units aligned along the

b direction. In effect, the Cu^{2+} ions form spin $S = 1/2$ chains along the b direction with dominant nearest-neighbor FM interactions and a weaker next-nearest-neighbor AFM coupling, resulting in a magnetically frustrated topology [13,14]. Recently, a detailed study of the magnetic interactions in linarite by combining magnetization measurements with ESR and NMR has been conducted [15]. The analysis of these data yields exchange constants of $J_1 \approx 100$ K and $J_2 \approx -36$ K, implying that $\alpha \approx -0.36$ lies close to the critical value of $-\frac{1}{4}$ (viz., close to a quantum critical point) [15]. The observation of a magnetically ordered state below $T_N = 2.8$ K implies the presence of residual interchain coupling 1 order of magnitude smaller than the intrachain coupling. Tentatively, the ordered phase has been discussed in terms of a possible helical ground state with an acute pitch angle [13]. A recent study of this material claiming multiferroicity has also been interpreted in terms of a helical magnetic ground state, with preliminary neutron-scattering data providing evidence for an incommensurate ordering vector of $\boldsymbol{k} \approx (0, 0.189, \frac{1}{2})$ [14,29].

Here, we establish linarite as a strongly frustrated quantum spin chain. By means of neutron scattering, we prove that as a consequence of frustration the magnetic ground state of linarite is of an elliptical helical nature. As a result of quantum fluctuations, the sizes of the moments are reduced compared to a free Cu^{2+} ion. Correspondingly, we demonstrate that the behavior in magnetic fields is also a consequence of the frustration by establishing a very rich magnetic phase diagram for magnetic fields applied along the chain direction.

For the neutron diffraction measurements, we used a single crystal of linarite from the batch studied in Ref. [15] with the dimensions $5 \times 2 \times 1$ mm^3. Neutron diffraction data were collected on the four-circle diffractometer D10 at the Institute Laue-Langevin with a neutron wavelength of $\lambda = 2.36$ Å at temperatures down to 1.8 K. A ^{3}He-position-sensitive detector was used to collect full data sets of both magnetic and nuclear reflections. To obtain the magnetic moments of the Cu atoms, the overall scale factor was determined from the crystal structure refinements using the program FULLPROF [30].

The thermodynamic measurements were performed on different crystalline pieces from the same batch as the neutron diffraction crystal. The experiments were conducted in the temperature range between 0.25 and 3 K and in magnetic fields from 0 to 12 T applied parallel to the crystallographic b and c axes as well as perpendicular to the bc plane by using various techniques. These include specific heat, the magnetocaloric effect, magnetization, susceptibility, magnetostriction, and thermal expansion. Here, we present results for measurements $B \parallel b$.

Using D10, broad sweeps of reciprocal space at 1.8 K reveal the existence of magnetic Bragg peaks. For example, in Fig. 1(a), the rocking scan of the $(0, 0.186, \frac{1}{2})$ peak at temperatures above and below T_N illustrates the appearance of magnetic intensity. From our experiments we found an incommensurate propagation vector of $\boldsymbol{k} = (0, 0.186, \frac{1}{2})$, which compares favorably with that from Ref. [29]. All of the 76 observed (25 unique) magnetic reflections were assigned indices according to $(hkl)_M = (hkl)_N \pm \boldsymbol{k}$. Magnetic intensities were found only for the satellites which were generated from the nuclear reflections $(hkl)_N$ with $k = 2n$. This shows that the magnetic moments of two neighboring copper atoms Cu1 and Cu2 (in the Wyckoff position $2a$ of $P2_1/m$) in $(0, 0, 0)$ and $(0, \frac{1}{2}, 0)$ are coupled parallel. The incommensurate vector component $k_y = 0.186$ along the b axis leads to a rotation angle between neighboring Cu atoms ($y = \frac{1}{2}$) along the b axis of 33.5°. We tried all possible spin configurations which are consistent with the crystal symmetry. First, we carried out the refinements by using a sine-wave modulated and a helical spin alignment. A considerably better fit ($R_F = 0.070$) was obtained by assuming an elliptical helix. In result, we have parameterized the moment evolution by the expression

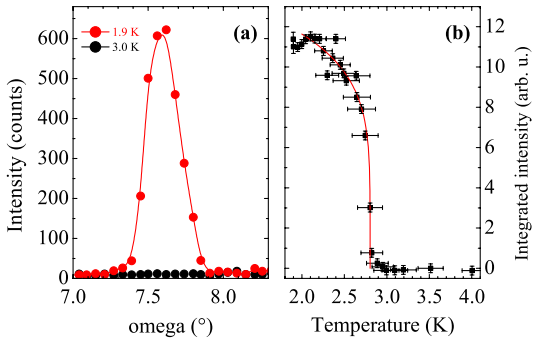

FIG. 1 (color online). (a) The magnetic peak $(0, 0.186, \frac{1}{2})$ of linarite at temperatures below and above T_N from rocking scans, with omega defining the angle of sample rotation. (b) Temperature dependence of the integrated intensity of the magnetic Bragg peak $(0, 0.186, \frac{1}{2})$.

$$\boldsymbol{\mu}_n = \mu_{xz} \cos(2\pi \boldsymbol{k} \cdot \boldsymbol{R}_n) \boldsymbol{u}_{xz} + \mu_y \sin(2\pi \boldsymbol{k} \cdot \boldsymbol{R}_n) \boldsymbol{v}_y. \quad (2)$$

Here, $\boldsymbol{R}_n$ represents a lattice point, and the unit vector $\boldsymbol{u}_{xz}$ defines the rotating plane in the ac plane and which is $-27(2)°$ off the a axis, while $\boldsymbol{v}_y$ is the unit vector along the b axis. The magnetic moment component $\mu_y = 0.833(10)\mu_B$ along the b axis is slightly larger than the component $\mu_{xz} = 0.638(15)\mu_B$ in the monoclinic ac plane. Thus, the rotating plane of the magnetic moments is almost parallel to $[1\ 0\ -1]$ and roughly perpendicular to the O4-O5 squares (Fig. 2). Altogether, our data disprove the spin alignment proposed in Ref. [29].

In Fig. 1(b), we plot the integrated intensity of the magnetic Bragg peak $(0, 0.186, \frac{1}{2})$ between 1.9 and 4 K. The data were fit in the range between 2 K and the Néel temperature T_N using $I(T) = A[(T_N - T)/T_N]^{2\beta}$. From

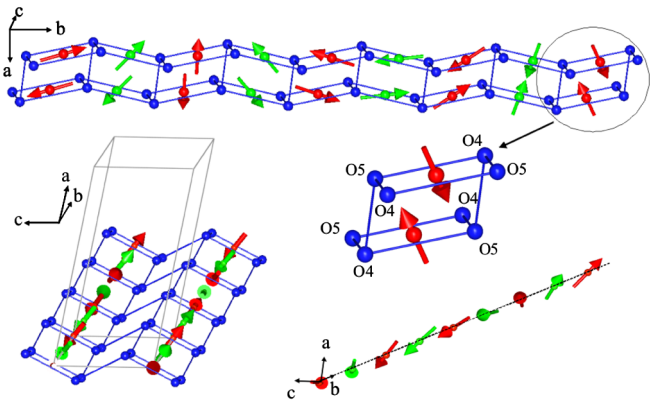

FIG. 2 (color online). The magnetic structure of linarite. Only the Cu^{2+} ions and the oxygen atoms O4 and O5 are shown. The two differently colored arrows symbolize the spins on the two copper sites: Cu1 (red) and Cu2 (green).

the fit we obtain the ordering temperature $T_N = 2.80$ K, which is in good agreement with the value obtained from bulk measurements. A critical exponent $\beta = 0.1(03)$ is derived from the fit, suggesting the phase transition at T_N to be of a second-order nature.

The zero-field helical ground state of linarite evolving along the b axis is the result of magnetic frustration. Hence, a complex magnetic behavior in fields $B \parallel b$ is expected. Experimentally, this is demonstrated in Fig. 3 with representative data from susceptibility χ and

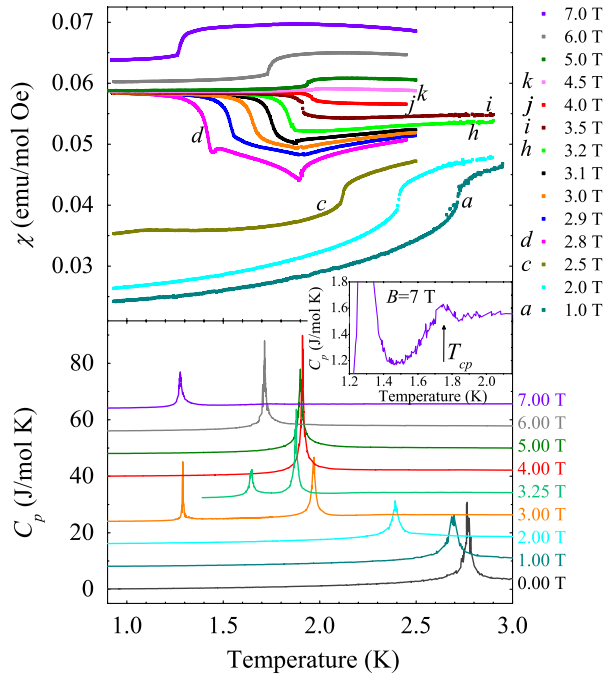

FIG. 3 (color online). Susceptibility (top) and specific heat (bottom; data in different fields shifted for clarity) for linarite with the magnetic field $B \parallel b$ axis. The inset shows the transition at T_{cp} in the specific-heat data for a magnetic field of 7 T.

specific-heat C_p measurements. The data indicate the presence of multiple magnetic phases, with a nonmonotonic evolution of transition temperatures with a field. Starting from low fields, the susceptibility shows a decrease of T_N with an increasing field up to $B = 2.5$ T. Between 2.8 and 3.2 T, a second transition is observed, with a weak (strong) field dependence of the upper (lower) transition temperature. Finally, for fields $B \geq 3.2$ T, again a single transition occurs, which shifts up to higher temperatures for fields up to 4.5 T and subsequently is suppressed.

Each transition is characterized by distinct features in $\chi(T)$ (Fig. 3). At low fields ($B \leq 2.5$ T), $\chi(T)$ exhibits a steplike increase at T_N (data sets a–c). At intermediate fields (2.8 T $\leq B <$ 3.2 T, sets d–h), the double transition is defined by a sharp drop for the lower (T_1) and a kink for the higher (T_2) transition. At high fields ($B \geq 3.2$ T), the transition temperature T_3 is determined from a drop in $\chi(T)$ up to ~4.5 T (sets i and j), while above this field (from k onwards) again a steplike increase denotes the transition.

The specific heat equally attests to the presence of multiple magnetic phases, showing anomalies in line with those observed in the susceptibility. Up to 2 T, T_N as well as the peak height decreases with an increasing field. Two anomalies (T_1 and T_2) are visible at 3 and 3.25 T. For fields up to 7 T, the specific-heat data again show only a single peak at T_3, with a maximum of T_3 at ~4.5 T. In addition, weak and broad specific-heat anomalies are detected at a temperature $T_{cp} > T_N$ in fields between 2 and 3 T and in high magnetic fields above the transition temperature T_3 (inset in Fig. 3).

The various transitions established from susceptibility and specific heat are also identified in the magnetization M, magnetocaloric effect (MCE), thermal expansion α, and magnetostriction β. Moreover, we find evidence for additional transitions or crossovers. First, below ~0.6 K in the magnetization a hysteretic transition occurs in field-sweep up vs down measurements [Fig. 4(a)]. From these data we obtain transition fields at B_s and B_e defining the hysteretic regime. Furthermore, in MCE—aside from anomalies upon crossing the phase transition line at T_3 in a field B_3—additional anomalies are observed at B_{cp} which correspond to the broad specific-heat anomaly of unknown nature in high magnetic fields [Fig. 4(b)]. By combining the different transition temperatures and fields from these data [31], we establish the magnetic phase diagram of linarite for $B \parallel b$ shown in Fig. 4(c).

The phase diagram in Fig. 4(c) contains five different phases or regions. Phase I represents the ground state of the elliptical magnetic helix, extending up to 2.8 K and 2.6 T. In region II (up to 0.63 K in fields of ~2.5–3 T), a magnetization hysteresis is observed. For field-sweep up the hysteresis consists of two steps at B_s and B_e, while for down sweeps there is only one step at B_s [Fig. 4(a)]. Thus,

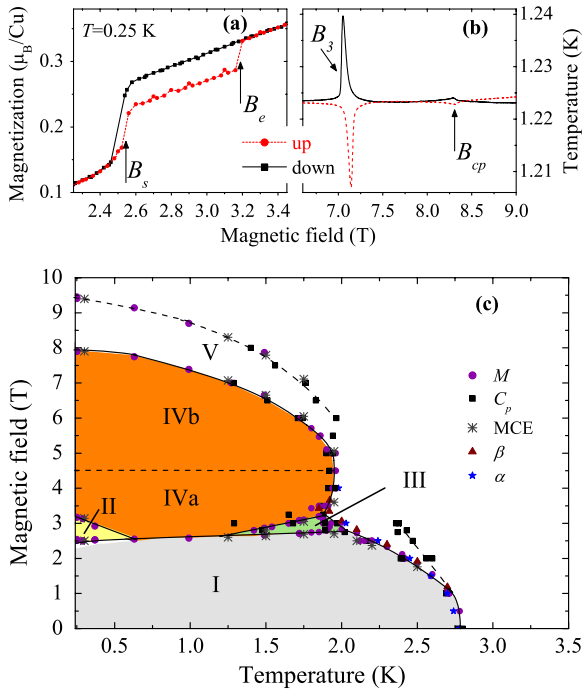

FIG. 4 (color online). (a) Detailed view of the magnetization of linarite with the hysteretic transition between the fields B_s and B_e and (b) the nonadiabatic MCE with the anomalies at the phase boundary (T_3, B_3) and the signatures at B_{cp}; for details, see the text. (c) Magnetic phase diagram of linarite for a magnetic field B along the b axis.

for down sweeps there is a direct transition from phase IV to I, implying that region II is not a distinct thermodynamic phase but a (possibly first-order) crossover from phase I to IV. Next, the signatures in C_p and $\chi(T)$ establish that there is a magnetic phase III wedged in between phases I and IV, with a multicritical point at ~1.25 K and 2.5 T. At higher fields, the magnetic phase IV below a phase transition at T_3 contains two regions IVa and IVb. Region IVa ranges up to about 4.5 T and has a negative slope in the susceptibility (Fig. 3) indicating a weakly ferromagnetic character, this likely from the canting of magnetic moments. Region IVb above ~4.5 T has a positive slope in $\chi(T)$ indicating a saturation of the weakly ferromagnetic moment. Phases I, III, and IV are long-range magnetically ordered states. The complex behavior observed in susceptibility and magnetization for phases III and IV possibly suggests that also these phases possess nontrivial ordering vectors. We speculate that the sequence of phases I-III-IV reflects reorientation processes of the spin spiral involving rotation of the helix or spin-flop transitions, as it was proposed for $LiCuVO_4$ [23]. Commonly, complex phase diagrams such as observed here for linarite are considered to reflect magnetic frustration as a result of the near degeneracy of different spin configurations.

Aside from the long-range ordered phases I, III, and IV, we have noted the existence of anomalies in C_p, M, and MCE at T_{cp}/B_{cp}, which defines a region V. The occurrence of anomalies in different thermodynamic quantities suggests that they are intrinsic to linarite. However, as they appear only as weak and broad features (see, for instance, the feature at T_{cp} in C_p in the inset in Fig. 3), we assume that short-range order effects take place here. In view of a qualitative resemblance to the behavior of $LiCuVO_4$, where nematic high field phases are proposed to exist [23], these features in linarite will be worthy of detailed study in the future.

In conclusion, we have determined the helical magnetic ground-state structure of linarite by means of neutron scattering. By use of thermodynamic measurements, we have established a rich magnetic phase diagram with multiple long-range ordered phases and possibly short-range ordered regions. Our results are understood within the framework of a frustrated one-dimensional spin $S = 1/2$ chain with ferromagnetic nearest-neighbor coupling $J_1 \approx 100$ K and an antiferromagnetic next-nearest-neighbor interaction $J_2 \approx -36$ K, which are predicted to generate helical states for the present parameter range. Long-range order is induced at temperatures $T_N \ll J_1, J_2$ as a result of a finite interchain coupling $J_{ic} \ll J_1, J_2$. Exchange anisotropy as discussed in Ref. [6] might then induce the small anisotropy of the helical state as exemplified by the elliptical modulation of the ordered magnetic moment. Altogether, linarite emerges as a model compound to study frustration in a quasi-one-dimensional magnet.

We acknowledge fruitful discussions with S.-L. Drechsler, S. Nishimoto, and R. Kuzian, as well as access to the experimental facilities of the Laboratory for Magnetic Measurements (LaMMB) at HZB. This work has partially been supported by the DFG under Contracts No. WO 1532/3-1 and No. SU229/10-1.

[1] U. Schollwöck, J. Richter, D. J. J. Farnell, and R. F. Bishop, *Quantum Magnetism*, Lect. Notes Phys. Vol. 645 (Springer, Heidelberg, 2004).
[2] C. Lacroix, P. Mendels, and F. Mila, *Introduction to Frustrated Magnetism*, Springer Ser. Solid-State Sci. Vol. 164 (Springer, Heidelberg, 2011).
[3] J. Sudan, A. Lüscher, and A. M. Läuchli, Phys. Rev. B **80**, 140402(R) (2009).
[4] F. Heidrich-Meisner, I. P. McCulloch, and A. K. Kolezhuk, Phys. Rev. B **80**, 144417 (2009).
[5] E. Plekhanov, A. Avella, and F. Mancini, Eur. Phys. J. B **77**, 381 (2010).
[6] R. O. Kuzian and S.-L. Drechsler, Phys. Rev. B **75**, 024401 (2007).
[7] M. Yamashita *et al.*, Nature Phys. **5**, 44 (2008).
[8] F. L. Pratt *et al.*, Nature (London) **471**, 612 (2011).
[9] H. Katsura, N. Nagaosa, and A. V. Balatsky, Phys. Rev. Lett. **95**, 057205 (2005).
[10] M. Mostovoy, Phys. Rev. Lett. **96**, 067601 (2006).
[11] S. Furukawa, M. Sato, and S. Onoda, Phys. Rev. Lett. **105**, 257205 (2010).
[12] K. C. Rule *et al.*, Phys. Rev. Lett. **100**, 117202 (2008).

[13] M. Baran *et al.*, Phys. Status Solidi C **3**, 220 (2006).
[14] Y. Yasui, M. Sato, and I. Terasaki, J. Phys. Soc. Jpn. **80**, 033707 (2011).
[15] A. U. B. Wolter *et al.*, Phys. Rev. B **85**, 014407 (2012).
[16] P. Mendels and F. Bert, J. Phys. Conf. Ser. **320**, 012004 (2011).
[17] T. Hamada *et al.*, J. Phys. Soc. Jpn. **57**, 1891 (1988).
[18] T. Tonegawa and I. Harada, J. Phys. Soc. Jpn. **58**, 2902 (1989).
[19] A. V. Chubukov, Phys. Rev. B **44**, 4693 (1991).
[20] T. Hikihara, L. Kecke, T. Momoi, and A. Furusaki, Phys. Rev. B **78**, 144404 (2008).
[21] M. E. Zhitomirsky and H. Tsunetsugu, Europhys. Lett. **92**, 37 001 (2010).
[22] B. J. Gibson *et al.*, Physica (Amsterdam) **350B**, e253 (2004).
[23] L. E. Svistov *et al.*, JETP Lett. **93**, 21 (2011).
[24] M. Hase *et al.*, Phys. Rev. B **70**, 104426 (2004).
[25] T. Masuda, A. Zheludev, A. Bush, M. Markina, and A. Vasiliev, Phys. Rev. Lett. **92**, 177201 (2004).
[26] S.-L. Drechsler *et al.*, Europhys. Lett. **73**, 83 (2006).
[27] S.-L. Drechsler *et al.*, Phys. Rev. Lett. **98**, 077202 (2007).
[28] H. Effenberger, Mineral. Petrol. **36**, 3 (1987).
[29] Y. Yasui, Y. Yanagisawa, M. Sato, and I. Terasaki, J. Phys. Conf. Ser. **320**, 012087 (2011).
[30] J. Rodriguez-Carvajal, Physica (Amsterdam) **192B**, 55 (1993).
[31] Transition fields B_s and B_e are also observed in MCE data; B_{cp} is identified in the magnetization (not shown).